DR. KOUROSH HONARMAND EBRAHIMI (Orcid ID : 0000-0001-6628-944X)

Received Date : 09-Feb-2020

Revised Date : 15-Mar-2020

Accepted Date : 16-Mar-2020

Article type : Hypothesis

# ddhCTP produced by the radical-SAM activity of RSAD2 (viperin) inhibits the NAD$^+$-dependent activity of enzymes to modulate metabolism

Kourosh Honarmand Ebrahimi*, Jane Vowles, Cathy Browne, James McCullagh, William S. James

Kourosh Honarmand Ebrahimi, Department of Chemistry, University of Oxford, Email: Kourosh.honarmandebrahimi@chem.ox.ac.uk

## Abstract

Radical S-adenosylmethionine (SAM) domain-containing protein 2 (RSAD2; viperin) is a key enzyme in innate immune responses that is highly expressed in response to viral infection and inflammatory stimuli in many cell types. Recently, it was found that RSAD2 catalyses transformation of cytidine triphosphate (CTP) to its analogue 3´-deoxy-3´,4´-didehydro-CTP (ddhCTP). The cellular function of this metabolite is unknown. Here, we analysed the extra- and intracellular metabolite levels in induced pluripotent stem cell (iPSC)-derived macrophages using

high resolution LC-MS/MS. The results together with biochemical assays and molecular docking simulations revealed that ddhCTP inhibits the $NAD^+$-dependent activity of enzymes including that of the house-keeping enzyme glyceraldehyde 3-phosphate dehydrogenase (GAPDH). We propose that ddhCTP regulates cellular metabolism in response to inflammatory stimuli such as viral infection, pointing to a broader function of RSAD2 than previously thought.

## Introduction

Radical S-adenosylmethionine domain-containing protein 2 (RSAD2), also known as viperin, is highly conserved from fungi to human. In humans, the protein is localized at the cytosolic face of the endoplasmic reticulum [1] and/or in lipid droplets via its N-terminus hydrophobic domain [2]. RSAD2 is a key enzyme of the innate immune response. Its expression is induced via interferon-dependent or -independent pathways [3]. It has been shown that RSAD2 is highly expressed in some types of cancer [4], in a subset of microglia with neurotoxic properties [5], and in response to viral infections in many cell types [6,7]. In addition to the widely studied broad-spectrum antiviral function of RSAD2 [8–15], emerging evidence suggests the enzyme may play a role in a range of different cellular processes. RSAD2 plays a role in optimal Th2 response [16], regulates thermogenesis in adipose tissue [17], is required for Golgi trafficking of TNF-α in activated microglia [18], and regulates chondrogenic differentiation via CXCL10 protein secretion [19]. The radical-SAM activity of RSAD2 can abolish metabolism of amino acids and mitochondrial respiration [20]. How RSAD2 can have such broad cellular functions is unknown. It has been discovered that the radical-SAM activity of vertebrate RSAD2 [21] and a fungal homologue of the enzyme [22] catalyses dehydration of cytidine triphosphate (CTP) to its analogue 3´-deoxy-3´,4´-didehydro-CTP (ddhCTP), while converting SAM to 5´-deoxyadenosine (5´-dA) (Figure 1). While human RSAD2 only catalyses transformation of CTP to ddhCTP, the fungal enzyme has substrate promiscuity [22]. Based on cell biological and biochemical assays, it is suggested that ddhCTP is a chain terminator of the RNA-dependent RNA polymerases (RdRps) of a number of flaviviruses [21]. This conclusion, however, was challenged after a re-evaluation of the data [20]. It is demonstrated that the reported data are consistent with the ddhCTP product of the radical-SAM activity of RSAD2 abolishing the cellular level of nucleotides and inhibiting mitochondrial activity [20]. These data suggest that ddhCTP modulates metabolism to restrict viral replication. It is not known how ddhCTP affects metabolism (Figure 1).

Here, using high-resolution mass spectrometry we analysed the extracellular metabolite levels of HEK293 cells overexpressing wild-type RSAD2 (WT-RSAD2) or an inactive variant of the enzyme (RSAD2-KO), and the extra- and intracellular metabolite levels of the iPSC-derived RSAD2-KO or WT-RSAD2-expressing macrophages (WT macrophages). Based on analysis of metabolite levels and biochemical assays, we demonstrate that ddhCTP inhibits the $NAD^+$-dependent activity of enzymes, including that of the house-keeping enzyme glyceraldehyde 3-phosphate dehydrogenase (GAPDH). Molecular docking simulations predict that ddhCTP binds to the $NAD^+$ binding pocket. We conclude that ddhCTP acts as a regulator of cellular metabolism upon inflammatory response. The results suggest a more general cellular role of the radical-SAM activity of RSAD2 than previously thought and provide an explanation for many data reported regarding the antiviral activity of RSAD2.

## Methods

***Chemicals.*** All chemicals were reagent grade and were purchased from Sigma Aldrich. S-adenosylmethionine salt (~75% purity) was purchased from Sigma Aldrich. The salt was dissolved in buffer (300 mM MOPS, 100 mM NaCl, pH 7.0) to a final concentration of 75 mM SAM. The solution was divided into aliquots of 20 µL and stored at a -20 ºC fridge. For each reaction a fresh aliquot of SAM was used. L-lactate dehydrogenase (LLDH) from rabbit muscle (10 KU), malic dehydrogenase (MDH) from bovine heart (10 KU), glyceraldehyde 3-phosphate dehydrogenase (GAPDH) from rabbit muscle (1KU), and phosphoglycerate kinase (PGK) from *S. cerevisiae* (2 KU) were purchased from Sigma Aldrich. The lyophilized powder of GAPDH was dissolved in 1 ml of phosphate buffer 50 mM, 300 mM NaCl, pH 7.6.

***Expression of RSAD2 and GFP in HEK293 cells.*** The construct for expression of wild-type RSAD2 (WT-RSAD2) was provided by Professor Peter Cresswell (Yale University). To create an inactive variant of human RSAD2 the highly conserved Ser300 and Tyr301 were replaced by alanine and phenylalanine, respectively. Mutations of these residues in a fungal homologue of the enzyme fully abolishes the activity [22]. To create the double variant (DM-RSAD2) of human RSAD2 the forward primer was 5' CCAGAAGATGAAAGACGCCTTCCTTATTCTGGATG 3' and the reverse primer was complementary to the forward primer. Quick-change site-direct mutagenesis kit was used and the insert of interest carrying the desired mutations was confirmed using sequencing (GENEWIZ). Transfection of HEK293 cells with the construct for expression of GFP, WT-RSAD2, or DM-RSAD2 was based on lipofectamine 2000 or Turbofect transfection reagent (ThermoFisher Scientific) according to the manufacturer protocol.

***Measuring extracellular metabolites using high-resolution mass spectrometry.*** The abundance of the extracellular metabolites in the growth medium before addition to cells and at 24 or 96 hr post transfection of HEK293 cells with GFP, WT-RSAD2, or DM-RSAD2 was measured using high-resolution liquid chromatography-mass spectrometry as explained previously [20].

***Generating RSAD2-KO iPSCs and deriving macrophages.*** Human iPSCs cell line SFC841-03-01 was obtained from the James Martin Stem Cell Facility, Sir William Dunn School of Pathology. The parental iPSC line SFC841-03-01 has been previously published [23]. It was originally derived from dermal fibroblasts from a disease-free donor recruited through the Oxford Parkinson's Disease Centre (participants were recruited to this study having given signed informed consent, which included derivation of hiPSC lines from skin biopsies (Ethics Committee: National Health Service, Health Research Authority, NRES Committee South Central, Berkshire, UK (REC 10/H0505/71)). Alt-R CRISPR-Cas9 system (Integrated DNA Technologies (IDT)) was applied as explained by the manufacturer. Mutagenic primers to target exon 3 of viperin (RSAD2) were gRNA (positive strand): 5´ UAUCCAAGGACCAAGCCCCU and gRNA (negative strand): 5´AAGCACUAAACCCUGUCCGC. This results in deletion of 269 base pairs from exon 3 of RSAD2 gene. Wild-type cells expressing RSAD2 were underwent the same procedure for CRISPR-Cas9 knockout except that the mutagenic primers were not added. This is to control for any unknown effect of the CRISPR-Cas9 procedure on cells. After picking more than 96 single colonies, PCR was used to identify wild-type cells and cell lines in which 269 base pairs from the exon 3 of RSAD2 were removed (Supplementary Figure 1). For PCR analysis, the forward primer was 5´AGAAGATGTCCAGAAGAAGCGG and the reverse primer was 5´AGGAAATCAGCAAAAGCGACC. SNP genotypic analysis were performed, and the results did not show any specific variation between RSAD2-KO and wild-type cells (Supplementary Figure 2). Two colonies were prepared and stored for subsequent studies. The resulting iPSC cells were used to generate embryoid bodies (EBs) using spinning method, which were then used to create factories to harvest macrophage precursors, which are differentiated to tissue-type macrophages as explained previously [24]. The physical properties and cell viability of EBs and macrophages derived from wild-type or RSAD2-KO iPSC cells were the same (Supplementary Figure 3). The macrophages derived from wild-type cells are referred to as wild-type (WT) throughout the manuscript. Macrophages were used for analysis of the extracellular and intracellular metabolite levels. Western blot analysis was performed as before [20].

***Preparation of samples from macrophages for untargeted metabolite analysis by negative ion mass spectrometry (LC-MS/MS).*** 50 µl of M-CSF, 45 µl LPS (1 mg/ml) and 30 µl of IFN-γ

(100 µg/ml) was added to 50 ml growth medium to prepare a stock solution of LPS and IFN-γ. When macrophages were ready, approximately 7 days after collection of macrophage precursors from EBs factories as described previously [24], fresh growth medium was added. Two hours later, 6 ml of growth medium was removed and 6 ml of the solution of LPS and IFN-γ was added. 72 hours after stimulation, 500 µl of growth medium was removed for analysis of extracellular metabolites and cells were collected for extraction of the intracellular metabolites. The aliquots of growth medium were filtered using 3 kDa Amicon Ultracentrifugal filters (Merk) and the flow through was used for analysis of extracellular metabolite levels. To extract intracellular metabolites, briefly, 50 ml of liquid nitrogen was added to fully cover the cells. Next, 500 µl cold methanol was added to extract the metabolites. Cells were removed with a cell scrapper and mixed in methanol. Subsequently, the mixture was centrifuged at 12,000 rpm for 5 minutes to remove cells debris. Concentration of DNA was measured in the supernatant using Nano-Drop™. The sample with the lowest concentration of DNA was used as reference and all other samples were diluted to this concentration. The extra- and intracellular metabolite levels were analysed using untargeted metabolite analysis by negative ion mass spectrometry (LC-MS/MS). Measurements and data analysis were performed as explained in details previously [25]. For data analysis, we used Progenesis QI software and compared the retention times and m/z ratios of different LC-MS/MS peaks with those of more than 600 in house standard metabolites or the m/z ratios of different peaks available from the human metabolome database (HMDB) website.

***Preparation of a mixture of ddhCTP and 5´-deoxyadenosine (5´-dA).*** We have confirmed that the thermostable fungal RSAD2 from *Thielavia terrestris* (TtRSAD2) can efficiently catalyses transformation of CTP to ddhCTP [22]. Thus, to prepare a mixture of ddhCTP and 5´-dA we used TtRSAD2. Wild-type TtRSAD2 was overexpressed in *E. coli* and purified as described before [26]. The buffer was exchanged to 50 mM phosphate buffer, 300 mM NaCl, pH 7.6 for performing enzymatic transformation of CTP to ddhCTP. Two reactions were prepared: ($R_1$) 500 µL TtRSAD2 (150 µM) + 20 µL SAM (75 mM) + 50 µL CTP (20 mM) + 5 µL phosphate buffer; ($R_2$) 2500 µL TtRSAD2 (150 µM) + 100 µL SAM (75 mM) + 250 µL CTP (20 mM) + 25 µL sodium dithionite (500 mM). CTP and sodium dithionite were prepared in 50 mM phosphate, 300 mM NaCl, pH 7.6. In reaction (i) the fungal enzyme will not convert CTP to ddhCTP because the reducing agent sodium dithionite was not added. Both reactions were incubated in an anaerobic glove box with $N_2$ atmosphere (Coy Laboratories, $O_2$ < 5 ppm) overnight (approximately 16 hrs). Subsequently, samples were subjected to centrifugation using 10 kDa Amicon Ultracentrifugal filters (Merk) to separate the enzyme. The flow-through was diluted to a final concentration of

approximately 1.5 mM ddhCTP and was used in further experiments to test the effect of ddhCTP and 5´-dA on activity of different $NAD^+$/NADH-dependent enzymes.

***Colorimetric assays for measuring activity of glyceraldehyde 3-phosphate dehydrogenase (GAPDH).*** Buffer was either phosphate 50 mM, 300 mM NaCl, pH 7.6 or Mops 50 mM, 20 mM NaCl, 10 mM phosphate, pH 7.6. 50 µL of GAPDH stock solution (as explained in chemicals section) was added to 50 ml of buffer to prepare a working solution of GADPH and 50 µL of phosphoglycerate kinase (PGK) was mixed with 10 ml of buffer to prepare a working solution of PGK for different assays. To measure activity of GAPDH using glyceraldehyde 3-phosphate (G3P) as substrate (forward reaction) two assays were used to measure steady-state kinetics of formation of $NAD^+$: (i) direct measurement of conversion of G3P by GAPDH, or (ii) coupling the activity of GAPDH, which converts G3P to 1,3-bisphosphoglycerate (1,3BPG), to the activity of PGK, which converts 1,3BPG to 3-phosphoglycerate. In the latter assay, activity of PGK allows near complete consumption of G3P by GAPDH. In assay (i) the following components were added to a quartz cuvette in order: 440 µL of working solution of GAPDH, 5 µL of stock $NAD^+$ (40 mM), and 10 or 50 µL of a solution containing ddhCTP and 5´-dA. To prepare the control reaction buffer was added instead of the solution containing ddhCTP and 5´-dA. To test if inhibition of enzymes is because of ddhCTP or 5´-dA, 5-10 µL solution of 5´-dA (10 mM) was added instead of the solution containing ddhCTP and 5´-dA. In each assay total volume of reaction was set 500 µL by addition of an aliquot of buffer if required. Each solution was added to a quartz cuvette (1 ml total volume and 1 cm path length) and the cuvette was placed in a UV-visible spectrometer. The absorbance was recorded at 340 nm for 1 min to establish a stable baseline. Subsequently, 2 or 5 µL of stock solution G3P (60 mM) was added to the solution and mixed rapidly (circa 3 seconds). Absorbance was followed at 340 nm for formation of NADH. In the second assay, first 5 µL of $NAD^+$ (40 mM) was mixed with 390 µL working solution of GAPDH. The mixture was added to a quartz cuvette, the cuvette was placed in a UV-visible spectrometer and the absorbance was recorded for 1-2 min to establish a stable baseline. Then, 5 µL G3P (60 mM) was added to the solution, mixed rapidly, and formation of NADH was followed until absorbance plateaued approximately after 3 min. Subsequently, a mixture of ($R_a$) 50 µL working solution of PGK + 50 µL phosphate buffer + 5 µL ADP (40 mM), or ($R_b$) a mixture of 50 µL working solution of PGK + 50 µL solution of ddhCTP and 5´-dA + 5 µL ADP (40 mM), or ($R_c$) a mixture of 50 µL working solution of PGK + 50 µL solution of CTP and SAM + 5 µL ADP (40 mM) was added. In each case, the solution was mixed rapidly, and absorbance was recorded at 340 nm for formation of NADH. To determine the inhibitory constant ($IC_{50}$ value) of ddhCTP and to measure activity of the reverse reaction, consumption of 1,3-biphosphoglycerate by GAPDH, the enzyme coupled

assay was used. For measuring the $IC_{50}$ value of ddhCTP, the volume of the mixture of ddhCTP+5´-dA added in $R_b$ was varied and the final volume was set to 500 µL by adding an aliquot of buffer. All experiments were repeated three times. All measurements were performed at room temperature, approximately 22 ºC. Rates of NADH formation or consumption were obtained from a linear fit to the data points recorded for the first 30 seconds and using a millimolar extinction coefficient ($\varepsilon_{340}$) of 6.22 mM.

***Colorimetric assay for measuring activity of L-lactate dehydrogenase (LLDH) or malic enzyme (MDH).*** The total volume of each reaction was 500 µL. To measure formation of NADH by catalytic activity of LLDH or MDH the following components were added to a 1 ml quartz cuvette (1 cm path length) in order: 470 or 490 µL of buffer, 5 µL of enzyme (LLDH or MDH), 5 µL of $NAD^+$ (40 mM stock), 0 or 20 µL of solution of (ddhCTP and 5´-dA). Next, the cuvette was placed in a UV-visible spectrometer and the absorbance was recorded at 340 nm to establish a stable baseline. After circa 1 min, 2 µL of a solution of 20 mM substrate (L-lactate or malate) was added to the cuvette. The solution was rapidly mixed and formation of NADH was followed at 340 nm. To measure the reverse reaction using LLDH, 20 mM stock solution of pyruvate was used as substrate and $NAD^+$ was replaced by NADH. Buffer was either phosphate 50 mM, 300 mM NaCl, pH 7.6 or Mops 50 mM, 20 mM NaCl, 10 mM phosphate, pH 7.6. All measurements were performed at room temperature, approximately 22 ºC. Rates of NADH formation or consumption were obtained as explained above.

**Molecular docking simulations.** The 3D model of ddhCTP was obtained using Chem3D software and was saved as a mol2 file. We used the X-ray crystal structure of GAPDH (PDB Code: 5C7O) and LLDH (PDB Code: 1T2F) solved in the presence of $NAD^+$. To perform the molecular docking, first the $NAD^+$ ligand was removed from the structure of each enzyme. Subsequently, the ligand-free structure and the 3D model of a ligand (ddhCTP, CTP, or ADP) were loaded into the SwissDock server [27]. Using this approach global molecular docking without bias toward a defined site is done. The structures with the highest Fullfitness rank and clustering numbers for a specific binding site were used for analysis of a ligand binding.

## Results and discussion

**Activity of RSAD2 in HEK293 cells inhibits $NAD^+$/NADH-dependent enzymatic reactions.** Previously, we overexpressed wild-type RSAD2 (WT-RSAD2), an inactive double variant of RSAD2 (DM-RSAD2), or green fluorescence protein (GFP) as a negative control in HEK293 cells. We analysed the extracellular metabolite levels 24- or 96-hours post-transfection of HEK293 cells

with a construct for expression of each protein [20]. We chose these time points because between 24-96 hours maximum intracellular amount of ddhCTP generated by the radical-SAM activity of WT-RSAD2 was reported [21]. The results confirmed that the cellular activity of RSAD2 abolished catabolism of different amino acids and led to an increase in the extracellular level of xanthine [20]. Further analysis of data revealed that the cellular activity of RSAD2 abolished extracellular levels of products of phenylalanine and tyrosine metabolism, namely phenylacetic acid and 4-hydroxyphenyllactic acid (Figure 2). A common step in metabolic pathways of amino acids, xanthine, phenylacetic acid, and 4-hydroxyphenyllactic acid is their dependency on the catalytic activity of $NAD^+$/NADH-dependent enzymes. Specifically, conversion of xanthine to uric acid requires the $NAD^+$-dependent activity of xanthine dehydrogenase and formation of phenylacetate requires the $NAD^+$-dependent activity of aldehyde dehydrogenases. Therefore, it is possible that the radical-SAM activity of RSAD2 inhibited the $NAD^+$/NADH-dependent enzymatic reactions leading to elevated extracellular level of xanthine and abolishing formation of phenylacetic acid and 4-hydroxyphenyllactic acid.

**Macrophages expressing RSAD2 have a lower activity of $NAD^+$-dependent enzymes.** To further test if the enzymatic activity of RSAD2 can inhibit $NAD^+$-dependent enzymatic reactions, we shifted to more physiologically relevant conditions. We knocked-out RSAD2 gene in iPSCs cells and derived macrophages as we have described and characterized before [24,28] (Methods). First, we confirmed that the RSAD2-KO cells were fully deficient in expressing the enzyme. To this end, we used western blot analysis and measured expression of RSAD2 before and after stimulation with a mixture of lipopolysaccharides (LPS) and IFN-γ. Before and after stimulation, only wild-type (WT) cells showed expression of RSAD2 (Figure 3A). The expression of protein in WT cells was significantly induced after stimulation with the mixture of LPS and IFN-γ (Figure 3A). The results confirmed that RSAD2-KO cells could not express the enzyme. Next, we investigated the difference between the extracellular metabolite levels of RSAD2-KO cells and those of WT cells, after stimulation with a mixture of LPS and IFN-γ (Methods). For several metabolites we noticed a significant difference ($p$ value $< 0.05$) between WT and RSAD2-KO cells (Supplementary Table 1). Among different metabolites, the most significant change was observed in the extracellular level of taurine (Figure 3B). It was 3.5-fold higher in RSAD2-KO cells as compared to WT cells. Formation of taurine directly requires $NAD^+$-dependent activity of hypotaurine dehydrogenase (HDH) (Figure 3B). Another metabolite whose extracellular level was 3-fold more in WT cells as compared to RSAD2-KO cells was 2-oxoglutarate (2-OG) (Figure 3C), which is converted by the $NAD^+$-dependent activity of 2-oxoglutarate dehydrogenase (2-OGDH)

to succinate. One explanation for these observations is that the enzymatic activity of RSAD2 can inhibit the $NAD^+$-dependent enzymatic reactions in macrophages to block formation of taurine and consumption of 2-OG. Besides taurine that has anti-inflammatory properties [29,30], we noticed that the level of another anti-inflammatory metabolite, namely guanosine [31,32], was higher in RSAD2-KO cells as compared to WT cells (Figure 3D). These data suggest to us that the cellular activity of RSAD2 in microphages induces a pro-inflammatory metabolic state.

**RSAD2-expressing macrophages produce ddhCTP and have a lower activity of GAPDH.** Next, we investigated the effect of RSAD2 expression on intracellular metabolite levels. We studied the difference between the intracellular metabolite levels in RSAD2-KO cells and those of WT cells (Methods). A list of metabolites whose levels were significantly different between WT and RSAD2-KO cells are given in Supplementary Table 2. The results revealed that in the RSAD2-KO cells catalytic transformation of CTP to ddhCTP did not occur (Figure 4A). No ddhCTP was detected in RSAD2-KO cells (Figure 4A) and the deoxyadenosine level, which is the sum of 2´-deoxyadenosine and 5´-deoxyadenosine (5´-dA) as measure by LC-MS/MS, was higher in WT cells as compared to RSAD2-KO cells (Figure 4A). Among the different metabolites detected, we noticed that the cellular level of glyceraldehyde 3-phosphate (G3P), which is consumed by the $NAD^+$-dependent activity of the house keeping enzyme GAPDH, was higher in WT cells as compared to RSAD2-KO cells (Figure 4B). Additionally, we found that the levels of sedoheptulose 7-phosphate and ribose 5-phosphate (Figure 4C), which are intermediates of pentose phosphate pathway (PPP), were higher in WT cells as compared to RSAD2-KO cells. This is consistent with inhibition of the glycolytic enzyme GAPDH and the increase in flux through PPP. Therefore, we conclude that the enzymatic activity of RSAD2 inhibited the $NAD^+$-dependent conversion of G3P to 1,3-biphosphoglycerate (1,3BPG) by the catalytic activity of GAPDH, which led to an increase in the intracellular level of G3P and consequently, the flux through PPP. Consistent with the results of extracellular metabolite levels of taurine and 2-OG, which suggested to us that the activity of RSAD2 inhibits the $NAD^+$-dependent activity of HDH and 2-OGDH (Figure 3), the intracellular level of taurine was lower (Figure 4D) and that of 2-OG was higher in WT cells as compared to RSAD2-KO cells (Supplementary Table 2). Therefore, the results of extra- and intracellular metabolite levels together, strongly suggest that the radical-SAM activity of RSAD2 inhibits the $NAD^+$-dependent activity of different enzymes.

**ddhCTP inhibits the NAD$^+$-dependent activity of GAPDH.** Guided by the results of metabolomics analysis, using biochemical assays we tested if the ddhCTP product of the radical-SAM activity of RSAD2 can inhibit the NAD$^+$-dependent activity of GAPDH (Figure 5A). First, we measured whether a mixture of the ddhCTP and 5´-dA products of the enzymatic activity of RSAD2 can inhibit the activity of GAPDH. To this end, we produced a mixture of ddhCTP and 5´-dA using RSAD2 [22] (Methods). NAD$^+$-dependent conversion of G3P to 1,3BPG by GAPDH was measured either directly or alternatively, using an enzyme-coupled assay (Methods). The results revealed that the mixture of ddhCTP and 5´-dA reduces NAD$^+$-dependent activity of GAPDH by approximately 3-fold (Figure 5A). To test whether this inhibition was due to the presence of ddhCTP or 5´-dA, we measured activity of GAPDH in the presence of synthetic 5´-dA. We observed that 5´-dA alone could not inhibit activity of GAPDH (Figure 5B). Therefore, we conclude that the ddhCTP generated by the radical-SAM activity of RSAD2 is necessary for the inhibition of GAPDH activity, either alone or in cooperation with the 5´-dA. Next, we tested if the reverse reaction catalysed by GAPDH, namely NADH-dependent conversion of 1,3BPG to G3P, was inhibited by ddhCTP (Supplementary Figure 4A). The results showed that ddhCTP could not inhibit the NADH-dependent conversion of 1,3BPG to G3P.

It has been proposed that ddhCTP acts as an effective chain terminator of viral RdRps [21]. Therefore, we sought to compare the efficiency of ddhCTP for inhibiting the activity of GAPDH with its reported efficiency as a viral RdRp chain terminator. We determined the half inhibitory concentration ($IC_{50}$ value) of ddhCTP as an inhibitor of GAPDH. We measured NAD$^+$-dependent conversion of G3P by GAPDH in the presence of physiologically relevant concentration of NAD$^+$, approximately 300-500 µM [21], by varying the concentration of ddhCTP (Supplementary Figure 4B). The resulting $IC_{50}$ value was 55.8 ± 0.2 µM. We compared this with $IC_{50}$ values reported for ddhCTP as a viral RdRps chain terminator [21] (Table 1). The comparison suggested that ddhCTP is 400-600,000 folds more effective at inhibiting GAPDH compared to its proposed inhibitory activity as a viral RdRp chain terminator (Table 1).

**ddhCTP inhibits the NAD$^+$-dependent activity of LLDH and MDH.** Our metabolomics data suggested that ddhCTP could potentially inhibit the activity of some other NAD$^+$-dependent reactions. Thus, we tested inhibition of the NAD$^+$-dependent activity of LLDH (Figure 5C) and malic enzyme (MDH) (Figure 5D and Supplementary Figure 5A). We observed that the mixture of ddhCTP and 5´-dA could efficiently block activity of both enzymes. Consistent with our observation that the 5´-dA alone did not inhibit NAD$^+$-dependent activity of GAPDH, we found that

the 5′-dA alone could not inhibit the $NAD^+$-dependent activity of LLDH (Supplementary Figure 5B). Next, we tested whether the reverse reaction catalysed by LLDH (Supplementary Figure 5C), namely NADH-dependent conversion of pyruvate was inhibited by ddhCTP. The results confirmed that ddhCTP could not inhibit the reverse reaction (Supplementary Figure 5C), consistent with our observation for GAPDH. Using biochemical assays, we found that ddhCTP in the presence of physiologically relevant amount of $NAD^+$, i.e. 500-300 µM [21], could inhibit the activity of $NAD^+$-dependent enzymes more than 2 folds (Figure 5). This level of inhibition measured by biochemical assays is consistent with metabolomics data. The extra- or intracellular levels of taurine, 2-OG, or G3P (Figures 3-4), whose formation or consumption requires the $NAD^+$-dependent activity of enzymes, was 1.5-3.5 folds different between WT and RSAD2-KO cells.

**ddhCTP binds to the $NAD^+$ binding pocket.** Next, we performed molecular docking simulations (Methods) to predict the binding pocket of ddhCTP in GAPDH and LLDH. First, we compared the $NAD^+$ binding pocket in the X-ray crystal structure of GAPDH (Figure 6A) or LLDH (Supplementary Figure 6A) with the predicted binding pocket of ddhCTP (Figure 6B and Supplementary Figure 6B). The results revealed that ddhCTP binds to the $NAD^+$ binding pocket in GAPDH and LLDH. Then, we predicted binding pocket of ADP (Figure 6C and Supplementary Figure 6C), which is a known inhibitor of GAPDH [33] and LLDH [34], or CTP (Figure 6D and Supplementary Figure 6D), which does not inhibit activity of the enzymes. We found that ADP binds to the binding pocket of $NAD^+$, while CTP binds elsewhere. The predicted change in the Gibbs free energy ($\Delta G$) was used to calculate the dissociation constant ($K_d$) of ddhCTP, CTP, or ADP (Table 2). It can be observed that the dissociation constants of ddhCTP and ADP is significantly less than that of CTP. These data strongly suggest that ddhCTP competes with $NAD^+$ and it can effectively inhibit $NAD^+$-dependent activity of GAPDH and LLDH. The predicted dissociation constant of ddhCTP for LLDH is 4-fold more than that for GAPDH. Therefore, ddhCTP has a higher affinity for the $NAD^+$ binding pocket in LLDH and should reduce the activity of LLDH more than GAPDH. This prediction is consistent with our biochemical data. In the presence of approximately 180 µM ddhCTP, the activity of GAPDH decreased circa 3-fold (Figure 5A), while in the presence of approximately 72 µM ddhCTP, the activity of LLDH dropped approximately 10-fold (Figure 5C).

## Conclusion

In summary, our analysis of extra- and intracellular metabolite levels, biochemical studies, and molecular docking simulations revealed that ddhCTP binds to the $NAD^+$ binding pocket and inhibits the $NAD^+$-dependent enzymatic reactions. Inhibition studies using the housekeeping enzyme GAPDH showed that unlike the previously reported inefficient role of ddhCTP as a viral chain terminator ($IC_{50}$ values of > 20-30 mM) (Table 1), inhibition of GAPDH by ddhCTP is much more efficient ($IC_{50}$ value of 0.055 mM) and occurs at physiologically relevant concentrations of ddhCTP and $NAD^+$. The difference in the $IC_{50}$ value of ddhCTP as an inhibitor of GAPDH and those reported for ddhCTP as a viral RdRps chain terminator is very large. Therefore, we contend that this difference is not linked to variations in assays and conditions.

Inhibition of $NAD^+$-dependent activity of enzymes will affect a range of downstream and/or upstream metabolic and signalling pathways. $NAD^+$ is a ubiquitous cofactor central to metabolism in all life forms, it is the source of ADP in ADP-ribosylation reactions [35], and it is the precursor for the cyclic ADP-ribose, a second messenger involved in $Ca^{2+}$ release and signalling [36,37]. Consequently, the radical-SAM activity of RSAD2 will have a wide range of downstream effects, which would impact many cellular processes. On the other hand, inhibition of the activity of GAPDH by the ddhCTP product of the radical-SAM activity of RSAD2 can affect upstream metabolic pathways. Specifically, it can increase the flux through the pentose phosphate pathway (PPP), which will increase the rate of regeneration of NADPH. In turn, this would increase the rate of reduction of glutathione disulphide (GSSG) to reduced glutathione (GSH), which protects the cells against damming effects of reactive oxygen species (ROS). Additionally, PPP is a metabolic redox sensor regulating transcription upon antioxidant response [38,39]. Therefore, it is possible that at least in some cell types like macrophages the cellular activity of RSAD2 provides a protective mechanism for the cells against the increase in the level of ROS under inflammatory response during viral infection [40] or other conditions. In some cell types, however, inhibition of $NAD^+$-dependent enzymatic reactions may cause an imbalance between energy and redox metabolism leading to cell death via apoptosis or other mechanisms to prevent spread of virus infection.

Based on our data, we propose a model for the cellular function of ddhCTP generated by the radical-SAM activity of RSAD2 (Figure 7): ddhCTP inhibits the $NAD^+$-dependent activity of several enzymes including that of GAPDH to modulate metabolism in response to pro-inflammatory stimuli such as viruses. How exactly this activity will restrict replication of different viruses needs to be further investigated. However, based on available data regarding the antiviral activity of RSAD2, different mechanisms can be postulated: (i) It is shown that the intracellular $NAD^+$ levels modulate TNF-α protein synthesis [41]. It is known that TNF has antiviral activity [42–

44] and it is observed that expression of TNF-α in RSAD2-KO cells decreases approximately two-fold [45]. These data together with our findings suggest that ddhCTP inhibits the $NAD^+$-dependent reactions to modulate the cellular level of TNF-α and restrict viral replication. (ii) Inhibiting $NAD^+$-dependent activity of enzymes by ddhCTP can increase the cellular amount of $NAD^+$, which is a precursor for ADP-ribosylation [35]. It is shown that ADP-ribosylation promotes 26S proteasome activity and degradation of proteins [46,47], and it has been observed that RSAD2 induces proteasome-dependent degradation of Zika virus non-structural protein NS3 to restrict viral replication [13]. Therefore, it is possible that inhibition of $NAD^+$-dependent reactions by ddhCTP induces ADP-ribosylation promoting degradation of viral proteins. (iii) ddhCTP does not efficiently chain terminate viral RdRps [20] (Supplementary Figure 7) and it interferes with mitochondrial respiration to restrict viral replication [20]. Inhibition of the $NAD^+$-dependent enzymes such as 2-OGDH, which catalyses transformation of 2-OG in TCA cycle, can reduce mitochondrial respiration and affects metabolism of nucleotides causing a reduction in viral replication. (iv) It is reported that the radical-SAM activity of RSAD2 reduces activity of β-oxidation pathway [17]. ddhCTP may inhibit the $NAD^+$-dependent activity of enzyme 3-hydroacyl-CoA dehydrogenase reducing the flux through the β-oxidation pathway.

In conclusion, inhibition of the $NAD^+$-dependent enzymatic reactions can have a broad cellular impact leading to the restriction of viral replication and other physiological or pathophysiological conditions. These impacts will potentially depend on the variation in the dissociation constants of ddhCTP for the $NAD^+$-binding pockets in proteins, the expression level of different enzymes, and the activity levels of various metabolic pathways.

## Acknowledgements

KHE is grateful to Professor Fraser Armstrong (University of Oxford, UK) for his generous support of the project. We are grateful to Dr James Wickens for his assistance in using LC-MS. We thank the James Martin Stem Cell Facility (Sir William Dunn School of Pathology, University of Oxford, UK) for supporting this work.

## Funding

The research on RSAD2 (viperin) was supported by an EMBO long-term fellowship to Dr Kourosh H. Ebrahimi (ALTF 157-2015) and an EPA Abraham Research Fund (RF259) to Professor William S. James and Dr Kourosh H. Ebrahimi. The research in the group of Professor James McCullagh is supported by Biotechnology and Biological Sciences Research Council (BBSRC) (BB/R013829/1) and Wellcome Institutional Strategic Support Fund (204826/Z/16/Z). iPSCs cells were supplied by the Oxford Parkinson's Disease Center (OPDC) study, funded by the Monument Trust Discovery Award from Parkinson's UK, a charity registered in England and Wales (2581970) and in Scotland (SC037554), with the support of the National Institute for Health Research (NIHR) Oxford Biomedical Research Center based at Oxford University Hospitals NHS Trust and University of Oxford, and the NIHR Comprehensive Local Research Network.

## Author contribution

KHE conceived the study; KHE designed and performed the experiments, and analysed data; JV and CB assisted in creating RSAD2-KO cells, WSJ suggested experiments, WSJ and JM provided support and facilities for experiments and discussed data; KHE wrote the manuscript with contribution from all the authors.

**References**

1 Hinson ER & Cresswell P (2009) The N-terminal amphipathic α-helix of viperin mediates localization to the cytosolic face of the endoplasmic reticulum and inhibits protein secretion,. *J. Biol. Chem.* **284**, 4705–4712.

2 Hinson ER & Cresswell P (2009) The antiviral protein, viperin, localizes to lipid droplets via its N-terminal amphipathic α-helix. *Proc. Natl. Acad. Sci.* **106**, 20452–20457.

3 Severa M, Coccia EM & Fitzgerald KA (2006) Toll-like receptor-dependent and -independent viperin gene expression and counter-regulation by PRDI-binding factor-1/BLIMP1. *J. Biol. Chem.* **281**, 26188–26195.

4 Rachidi SM, Qin T, Sun S, Zheng WJ & Li Z (2013) Molecular Profiling of Multiple Human Cancers Defines an Inflammatory Cancer-Associated Molecular Pattern and Uncovers KPNA2 as a Uniform Poor Prognostic Cancer Marker. *PLoS One* **9**, e57911.

5 Mathys H, Adaikkan C, Gao F, Young JZ, Manet E, Hemberg M, De Jager PL, Rnsohoff RM, Regev A & Tsai L-H (2017) Temporal Tracking of Microglia Activation in Neurodegeneration at Single-Cell Resolution. *Cell Rep.* **21**, 366–380.

6 Seo J-Y, Yaneva R & Cresswell P (2011) Viperin: a multifunctional, interferon-inducible protein that regulates viprus replication. *Cell Host Microbe* **10**, 534–539.

7 Severa M, Coccia EM & Fitzgerald KA (2006) Toll-like receptor-dependent and -independent viperin gene expression and counter-regulation by PRDI-binding factor-1/BLIMP1. *J. Biol. Chem.* **281**, 26188–26195.

8 Wang S, Wu X, Pan T, Song W, Wang Y, Zhang F & Yuan Z (2012) Viperin inhibits hepatitis C virus replication by interfering with binding of NS5A to host protein hVAP-33. *J. Gen. Virol.* **93**, 83–92.

9 Seo J-Y, Yaneva R, Hinson ER & Cresswell P (2011) Human cytomegalovirus directly induces the antiviral protein viperin to enhance infectivity. *Science (80-. ).* **332**, 1093–1097.

10 Van der Hoek KH, Eyre NS, Shue B, Khantisitthiporn O, Glab-Ampi K, Carr JM, Gartner MJ, Jolly LA, Thomas PQ, Adikusuma F, Jankovic-Karasoulos T, Roberts CT, Helbig KJ & Beard MR (2017) Viperin is an important host restriction factor in control of Zika virus infection. *Sci. Rep.* **7**, 4475.

11 Helbig KJ, Eyr NS, Yip E, Narayana S, Li K, Fiches G, McCartney EM, Jangra RK, Lemon SM

& Beard MR (2011) The antiviral protein viperin inhibits hepatitis C virus replication via interaction with nonstructural protein 5A. *Hepatology* **54**, 1506–1517.

12 Seo J-Y & Cresswell P (2013) Viperin Regulates Cellular Lipid Metabolism during Human Cytomegalovirus Infection. *PloS Pathog.* **9**, e1003497.

13 Panayiotou C, Lindqvist R, Kurhade C, Vonderstein K, Pasto J, Edlund K, Upadhyay AS & Overby AK (2018) Viperin Restricts Zika Virus and Tick-Borne Encephalitis Virus Replication by Targeting NS3 for Proteasomal Degradation. *J. Virol.* **92**, e02054-17.

14 Ghosh S, Patel AM, Grunkemeyer TJ, Dumbrepatil AB, Zegalia KA, Kennedy RT & Marsh ENG (2020) Interactions between viperin, vesicle-associated membrane protein A and Hepatitis C virus protein NS5A modulate viperin activity and NS5A degradation. *Biochemistry* **59**, 780–789.

15 Dumbrepatil AB, Ghosh S, Zegalia KA, Malec PA, Hoff JD, Kennedy RT & Marsh ENG (2019) Viperin interacts with the kinase IRAK1 and the E3 ubiquitin ligase TRAF6, coupling innate immune signaling to antiviral ribonucleotide synthesis. *J. Biol. Chem.* **10.1074/jb**.

16 Qiu L-Q, Cresswell P & Chin K-C (2009) Viperin is required for optimal Th2 responses and T-cell receptor–mediated activation of NF-kB and AP-1. *Blood* **113**, 3520–3529.

17 Eom J, Kim JJ, Yoon SG, Jeong H, Son S, Lee JB, Yoo J, Seo HJ, Cho Y, Kim KS, Choi KM, Kim IY, Lee HY, Nam KT, Cresswell P, Seong JK & Seo JY (2019) Intrinsic expression of viperin regulates thermogenesis in adipose tissues. *Proc. Natl. Acad. Sci.* **116**, 17419–17428.

18 Chung SE, Chung H & Bae H (2011) RSAD2 is a key requirement for Golgi trafficking of TNF-alpha in activated Microglia. *J. Immunol.* **186**, 1176.216.

19 Steinbusch MMF, Caron MMJ, Surtel DAM, van den Akker GGH, van Dijk PJ, Friedrich F, Zabel B, van Rhijn LW, Peffers MJ & Welting TJM (2019) The antiviral protein viperin regulates chondrogenic differentiation via CXCL10 protein secretion. *J. Biol. Chem.* **294**, 5121–5136.

20 Honarmand Ebrahimi K, Howie D, Rowbotham J, McCullagh J, Armstrong F & James WS (2020) Viperin, through its radical-SAM activity, depletes cellular nucleotide pools and interferes with mitochondrial metabolism to inhibit viral replication. *FEBS Lett.*

21 Gizzi AS, Grove TL, Arnold JJ, Jose J, Jangra RK, Garforth SJ, Du Q, Cahill SM, Dulyaninova NG, Love JD, Chandran K, Brenick AR, Cameron CE & Almo SC (2018) A naturally

occurring antiviral ribonucleotide encoded by the human genome. *Nature* **558**, 610–614.

22 Honarmand Ebrahimi K, Rowbotham J, McCullagh J & James WS (2020) Mechanism of diol dehydration by a promiscuous radical-SAM enzyme homologue of the antiviral enzyme viperin (RSAD2). *ChemBioChem*, 10.1002/cbic.201900776.

23 Dafinca R, Scaber J, Ababneh N, Lalic T, Weir G, Christian H, Vowles J, Douglas AG, Fletcher-Jones A, Browne C, Nakanishi M, Turner MR, Wade-Martins R, Cowley SA & Talbot K (2016) C9orf72 Hexanucleotide Expansions Are Associated with Altered Endoplasmic Reticulum Calcium Homeostasis and Stress Granule Formation in Induced Pluripotent Stem Cell-Derived Neurons from Patients with Amyotrophic Lateral Sclerosis and Frontotemporal Demen. *Stem Cells* **34**, 2063–2078.

24 van Wilgenburg B, Browne C, Vowles J & Cowley SA (2013) Efficient, long term production of monocytes-derived macrophages from human pluripotent stem cells under partly-defined and fully-defined conditions. *PLoS One* **8**, e71098.

25 Alldritt I, Whitham-Agut B, Sipin M, Studholme J, Trentacoste A, Tripp JA, Cappai MG, Ditchfield P, Deviese T, Hedges REM & McCullagh JSO (2019) Metabolomics reveals diet-derived plant polyphenols accumulate in physiological bone. *Sci. Rep.* **9**, 8047.

26 Honarmand Ebrahimi K, Carr SB, McCullagh J, Wickens J, Rees NH, Cantley J & Armstrong F (2017) The radical-SAM enzyme Viperin catalyzes reductive addition of a 5′-deoxyadenosyl radical to UDP-glucose in vitro. *FEBS Lett.* **591**, 2394–2405.

27 Grosdidier A, Zoete V & Michielin O (2007) EADock: Docking of small molecules into protein active sites with a multiobjective evolutionary optimization. *Proteins*, 1010–1025.

28 Haenseler W, Sansom SN, Buchrieser J, Newey SE, Moore CS, Nicholls FJ, Chintawar S, Schnell C, Antel JP, Allen ND, Cader MZ, Wade-Martins R, James WS & Cowley SA (2017) A Highly Efficient Human Pluripotent Stem Cell Microglia Model Displays a Neuronal-Co-culture-Specific Expression Profile and Inflammatory Response. *Stem Cell Reports* **8**, 1727–1742.

29 Schuller-Levis GB & Park E (2003) Taurine: new implications for an old amino acid. *FEMS Microbiol. Lett.* **226**, 195–202.

30 Nakajima Y, Osuka K, Seki Y, Gupta RC, Hara M, Takayasu M & Wakabayashi T (2010) Taurine Reduces Inflammatory Responses after Spinal Cord Injury. *J. Neurotrauma* **27**, 403–410.

31 Dal-Cim T, Ludka FK, Martins WC, Reginato C, Parada E, Egea J, Lopez MG & Tasca CI (2013) Guanosine controls inflammatory pathways to afford neuroprotection of hippocampal slices under oxygen and glucose deprivation conditions. *J. Neurochem.* **126**, 437–450.

32 Bellaver B, Souza DG, Bobermin LD, Goncalves CA, Souza DO & Quincozes-Santos A (2015) Guanosine inhibits LPS-induced pro-inflammatory response and oxidative stress in hippocampal astrocytes through the heme oxygenase-1 pathway. *Purinergic Signal.* **11**, 571–580.

33 Maurer J, Bovo F, Gomes E, Loureiro H, Stevan F, Zawadzki-Baggio S & Nakano M (2015) Kinetic Data of D-Glyceraldehyde-3-Phosphate Dehydrogenase from HeLa Cells. *Curr. Enzym. Inhib.* **11**, 124–131.

34 Zhao R, Zheng S, Duan C, Liu F, Yang L & Huo G (2013) NAD-dependent lactate dehydrogenase catalyses the first step in respiratory utilization of lactate by Lactococcus lactis. *FEBS Open Bio* **3**, 379–386.

35 Corda D & Girolamo MD (2003) Functional aspects of protein mono-ADP-ribosylation. *EMBO J.* **22**, 1953–1958.

36 Kim H, Jacobson EL & Jacobson MK (1993) Synthesis and degradation of cyclic ADP-ribose by NAD glycohydrolases. *Science (80-. ).* **261**, 1330–1333.

37 Guse AH, da Silva CP, Berg I, Skapenko AL, Weber K, Heyer P, Hohenegger M, Ashamu GA, Schulze-Koops H, Potter BVL & Mayr GW (1999) Regulation of calcium signalling in T lymphocytes by the second messenger cyclic ADP-ribose. *Nature* **398**, 70–73.

38 Kruger A, Gruning NM, Wamelink MMC, Kerick M, Kirpy A, Parkhomchuk D & Bluemlein K (2011) The Pentose Phosphate Pathway Is a Metabolic Redox Sensor and Regulates Transcription During the Antioxidant Response. *Antioxid. Redox Signal.* **15**, 311–324.

39 Grant CM (2008) Metabolic reconfiguration is a regulated response to oxidative stress. *J. Biol.* **7**, l.

40 Schwarz KB (1996) Oxidative stress during viral infection: A review. *Free Radic. Biol. Med.* **21**, 641–649.

41 Van Gool F, Galli M, Gueydan C, Kruys V, Bedalov A, Mostoslavsky R, Alt FW, Smedt TD & Leo O (2009) Intracellular NAD levels regulate TNF-α protein synthesis in a sirtuin-dependent manner. *Nat. Med.* **15**, 206–210.

42 Ruby J, Bluethmann H & Peschon JJ (1997) Antiviral Activity of Tumor Necrosis Factor (TNF) Is Mediated via p55 and p75 TNF Receptors. *J. Exp. Med.* **186**, 1591–156.

43 Wong GH, Tartaglia LA, Lee MS & Goeddel D V. (1992) Antiviral activity of tumor necrosis factor is signaled through the 55-kDa type I TNF receptor. *J. Immunol.* **149**, 3350–3353.

44 Aldridge JR, Moseley CE, Boltz DA, Negovetich NJ, Reynolds C, Franks J, Brown SA, Doherty PC, Webster RG & Thomas PG (2009) TNF/iNOS-producing dendritic cells are the necessary evil of lethal influenza virus infection. *Proc. Natl. Acad. Sci.* **106**, 5306–5311.

45 Eom J, Yoo J, Kim JJ, Lee JB, Choi W, Park CG & Seo JY (2018) Viperin Deficiency Promotes Polarization of Macrophages and Secretion of M1 and M2 Cytokines. *Immune Netw.* **18**, e32.

46 Ullrich O, Reinheckel T, Sitte N, Hass R, Grune T & Davies KJA (1999) Poly-ADP ribose polymerase activates nuclear proteasome to degrade oxidatively damaged histones. *Proc. Natl. Acad. Sci.* **96**, 6223–6228.

47 Cho-Park PF & Steller H (2013) Proteasome Regulation by ADP-Ribosylation. *Cell* **153**, 614–627.

**Table 1.** Comparison of the $IC_{50}$ value of ddhCTP for inhibition of GAPDH with those of ddhCTP as chain terminator of RdRps.

| Enzyme | $IC_{50}$ values (μM) | Reference |
|---|---|---|
| **GAPDH** | 55 | This work |
| **DV RdRp** | 30000 | [21] |
| **WNV RdRp** | 20000 | [21] |
| **HRV-C RdRp** | 3000000 | [21] |
| **PV RdRp** | > 30000000 | [21] |

DV, dengue virus; WNV, West Nile virus; HRV-C, human rhinoviruses C; PV, poliovirus. The $IC_{50}$ value for inhibition of GAPDH by ddhCTP was obtained in the presence of physiologically relevant concentration of $NAD^+$, i.e. 400 μM. The $IC_{50}$ values for RdRp of different flaviviruses were estimated.

**Table 2.** Comparison of the predicted $\Delta G$ and dissociation constants ($K_d$) of ddhCTP, CTP, and ADP.

| Enzyme | Ligand | $\Delta G$ (kcal/mol) | $K_d$ (nM) |
|---|---|---|---|
| GAPDH | ddhCTP | -9.79 | 65.9 |
| | CTP | -7.54 | 2949.8 |
| | ADP | -8.99 | 254.85 |
| LLDH | ddhCTP | -10.59 | 17.0 |
| | CTP | -9.12 | 204.6 |
| | ADP | -9.26 | 161 |

$\Delta G$ (kcal/mol) was obtained from molecular docking simulation. $K_d$ was calculated from the Gibbs free energy: $\Delta G = RTlnK_d$, in which R is the universal gas constant and equal to 1.987 (kcal/mol·K) and T is temperature (K) and was assumed to be 298 K.

**Figure 1.** The radical-SAM activity of RSAD2 modulates cellular metabolism. The radical-SAM activity of RSAD2 catalyses transformation of CTP to ddhCTP. In this process SAM is converted to 5´-dA. It has been shown that this activity interferes with metabolism to restrict viral replication [20]. The underlying molecular details of this effect of ddhCTP is unknown. C, cytosine.

**Figure 2.** Expression of RSAD2 in HEK293 cells abolished extracellular levels of metabolites requiring activity of $NAD^+$/NADH- dependent enzymes. The extracellular levels of (A) phenylacetic acid and (B) 4-hydroxyphenyllactic acid were lower for HEK293 cells expressing WT-RSAD2 as compared to those for cells expressing inactive enzymes, i.e. GFP or an inactive variant of RSAD2 (DM-RSAD2). Extracellular metabolite levels were measured 24 or 96 hr post transfection of HEK293 cells with GFP, WT-RSAD2, or the inactive DM-RSAD2. The results are plotted relative to the amount of metabolite in the growth medium before addition to the cells. Data are average of three independent biological replicates ± standard deviation.

**Figure 3.** WT macrophages have a lower activity of the $NAD^+$-dependent enzymes. (A) Western blot analysis of expression of RSAD2 in wild-type (WT) or RSAD2-KO (KO) macrophages. Cells were treated for 72 hr with a mixture of IFN-γ and LPS (+) or with no stimuli. (B-D) WT or RSAD2-KO cells were stimulated with a mixture of LPS and IFN-γ. WT Cells showed a lower level of (B) taurine and an elevated level of (C) 2-oxoglutarate. (D) The extracellular level of anti-inflammatory metabolite guanosine was lower for WT cells as compare to RSAD-KO cells. The data are plotted as a % of the level of metabolite in WT cells. Data are average of three independent biological replicates ± standard deviation.

**Figure 4.** WT macrophages produce ddhCTP and have a lower GAPDH activity. (A) Expression of RSAD2 leads to formation of ddhCTP and 5´-dA in iPSCs-derived macrophages. (B) Cells expressing WT-RSAD2 had elevated levels of the glycolytic metabolite G3P and (C) the metabolites of PPP including sedoheptulose 7-phosphate and ribose 5-phosphate. (D) Cells expressing WT-RSAD2 had a lower intracellular level of the anti-inflammatory metabolite taurine. The data are plotted as a % of the level of metabolite in WT macrophages. Data are average of three independent biological replicates ± standard deviation. Cells were stimulated with a mixture of LPS and IFN-γ.

**Figure 5.** Steady-state kinetics of inhibition of the $NAD^+$-dependent activity of GAPDH, LLDH, and MDH by ddhCTP. (A) Steady-state progress curves and initial rates of formation of NADH due to conversion of G3P by GAPDH were measured using the enzyme-coupled assay as explained in the methods. (i) Addition of G3P (final concentration of 600 µM) to a solution containing GAPDH and $NAD^+$ (final concentration of 400 µM). (ii) Addition of a mixture of PGK and ADP (final concentration of 400 µM) (control), PGK, ADP, and ddhCTP+5´-dA, or PGK, ADP, and CTP+SAM. Addition of the second solution (ii) results in conversion of the 1,3-biphosphoglycerate (1,3BPG) product of the enzymatic activity of GAPDH to 3-phosphoglycerate. Consequently, the reaction is pushed towards near complete conversion of G3P to 1,3BPG by GAPDH. (B) Steady-state initial rate of formation of NADH by GAPDH in the presence of ddhCTP and 5´-dA or 5´-dA alone as compared to control. (C) Steady-state progress curves and rate of formation of NADH by the catalytic activity of LLDH in the presence of a mixture of ddhCTP and 5´-dA as compared to control. (D) Rate of formation of NADH by the catalytic activity of MDH in the presence of a mixture of ddhCTP and 5´-dA as compared to control. Concentration of ddhCTP was approximately (A) 180 µM, (B) 36 µM, and (C-D) 72 µM. The control reaction contains only the enzymes and substrates.

**Figure 6.** ddhCTP binds to the $NAD^+$ binding pocket. (A) Binding pocket of $NAD^+$ in the X-ray crystal structure of GAPDH (PDB Code: 5C7O) is compared to the predicted binding pocket of (B) ddhCTP, (C) ADP, or (D) CTP. Binding pocket of ddhCTP, ADP, or CTP was predicted using molecular docking simulation with the ligand-free X-ray crystal structure of GAPDH (PDB Code: 5C7O).

**Figure 7.** The proposed model for the cellular function of ddhCTP generated by the radical-SAM activity of RSAD2 (viperin). ddhCTP blocks the catalytic activity of $NAD^+$-dependent enzymatic reactions such as the conversion of G3P to 1,3BPG by GAPDH. As a result, the flux through pentose phosphate pathway increases. This increases the rate of regeneration of NADPH, which is essential for redox metabolism and reduction of glutathione disulfide (GSSG) by glutathione disulfide reductase (GSR) to glutathione (GSH). Additionally, rate of consumption of $NAD^+$ will be reduced, which would alter many downstream signalling pathways for example ADP-ribosylation or formation of cyclic ADP-ribose.

Figure 1

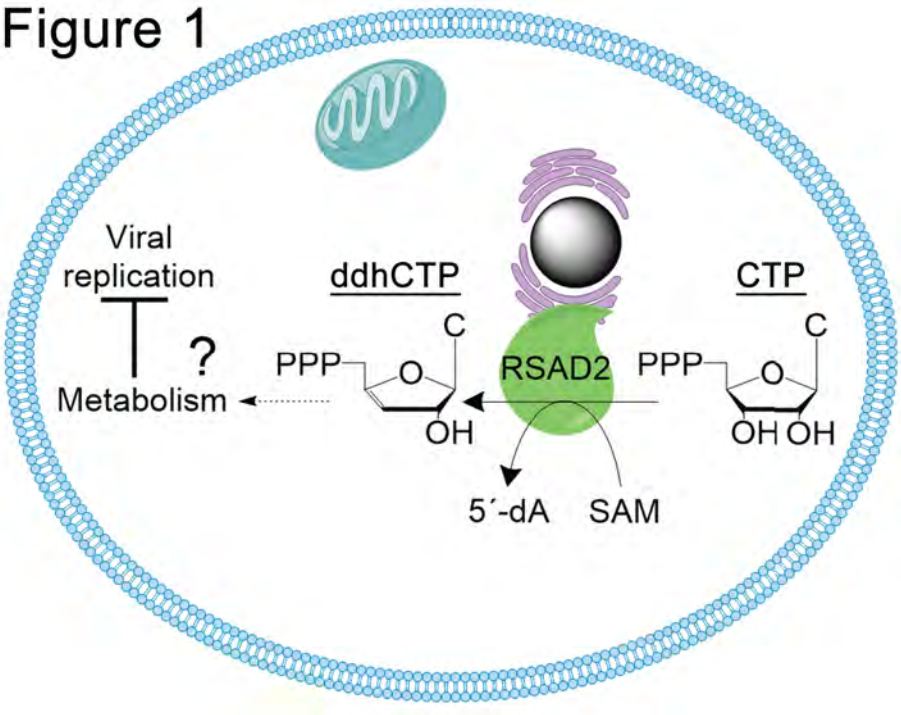


feb2_13778_f1.tif

Figure 2

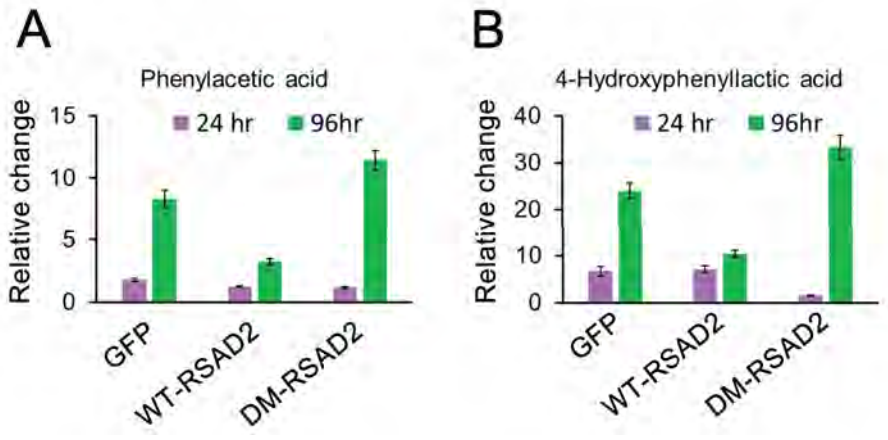


feb2_13778_f2.tif

Figure 3

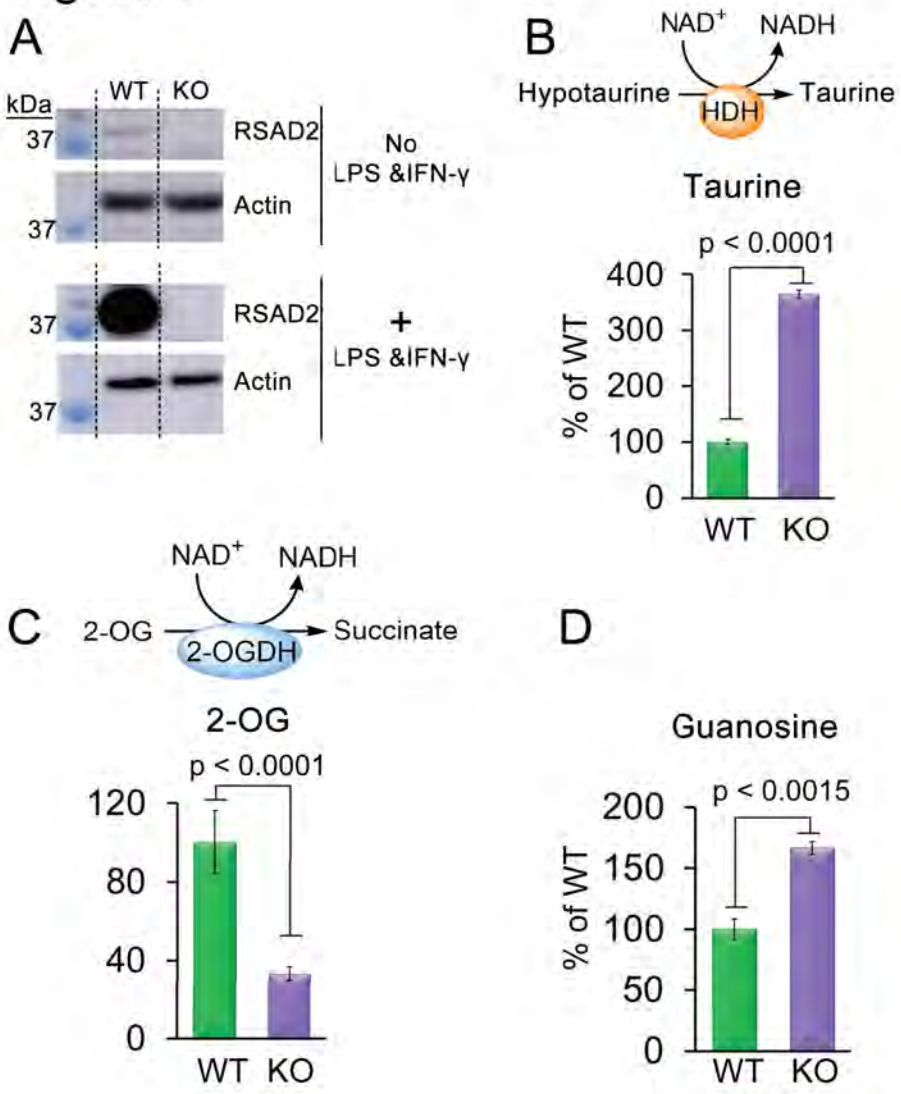


feb2_13778_f3.tif

Figure 4

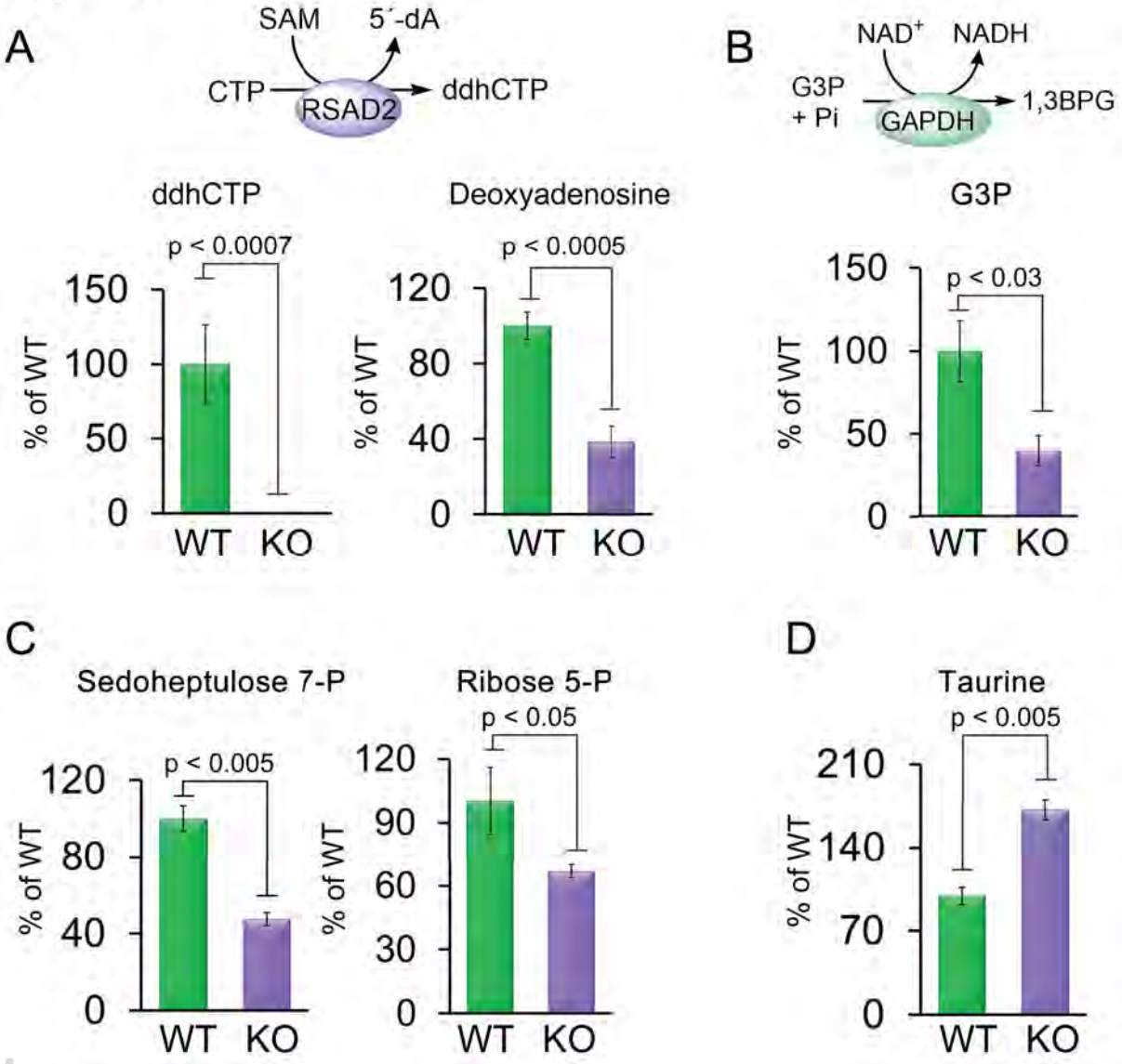


feb2_13778_f4.tif

Figure 5

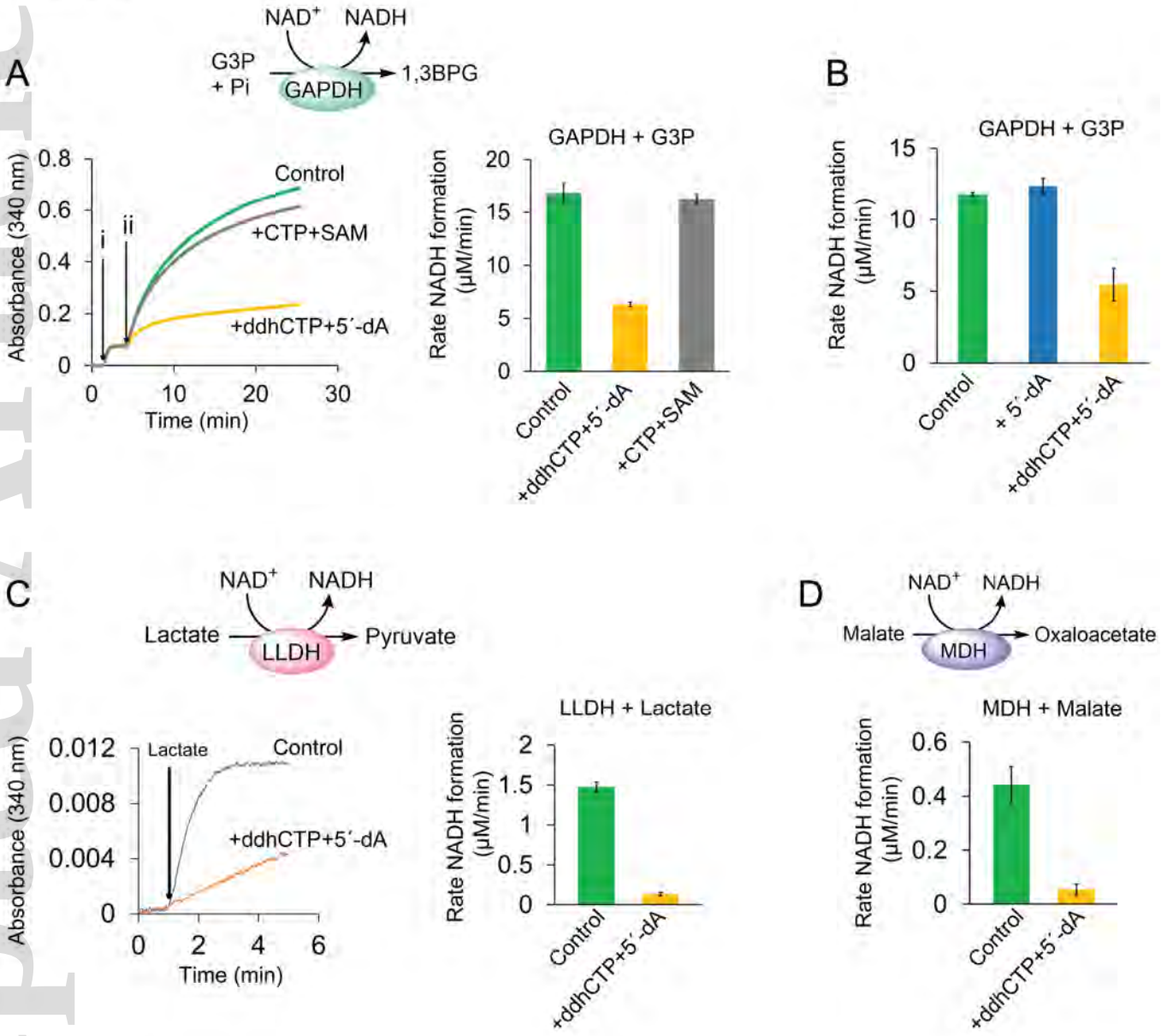


feb2_13778_f5.tif

Figure 6

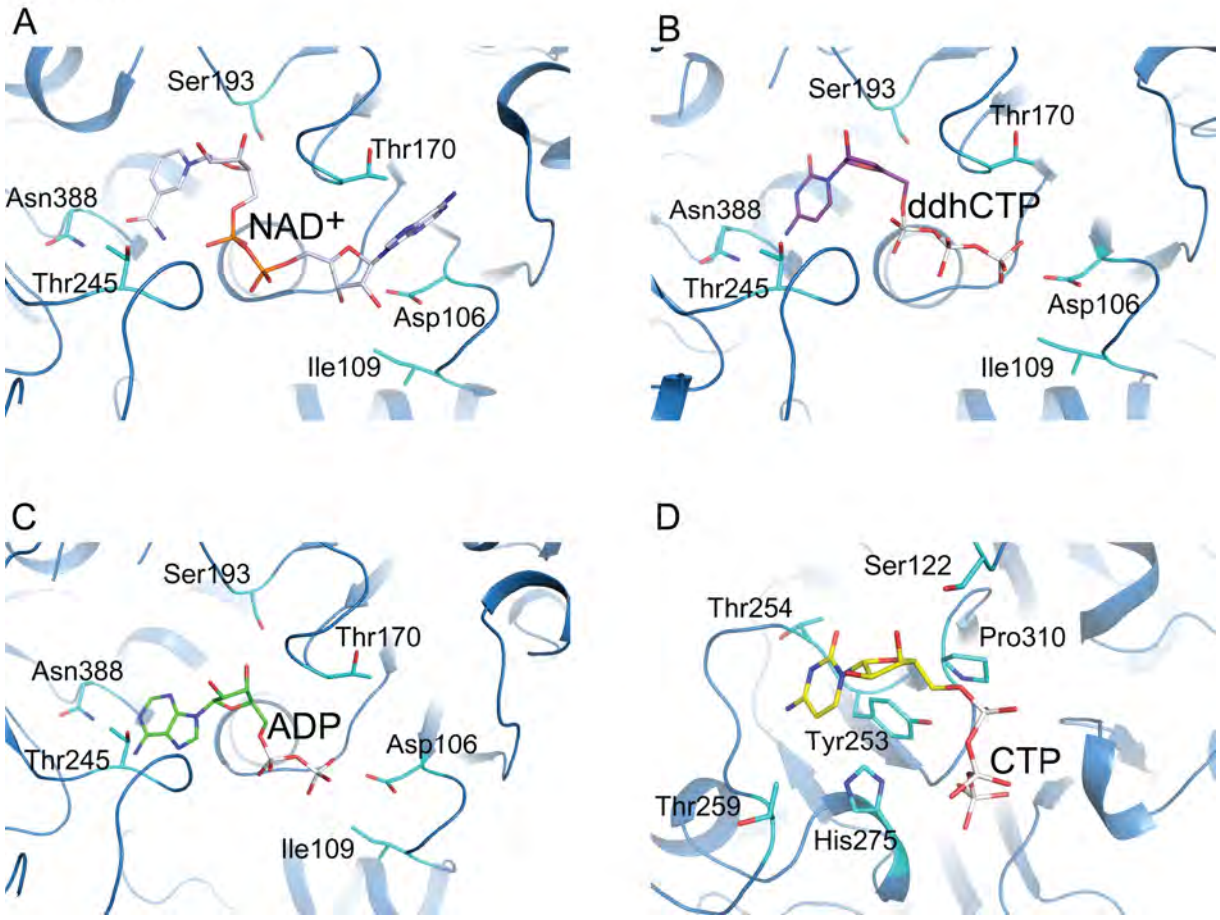


feb2_13778_f6.tif

Figure 7

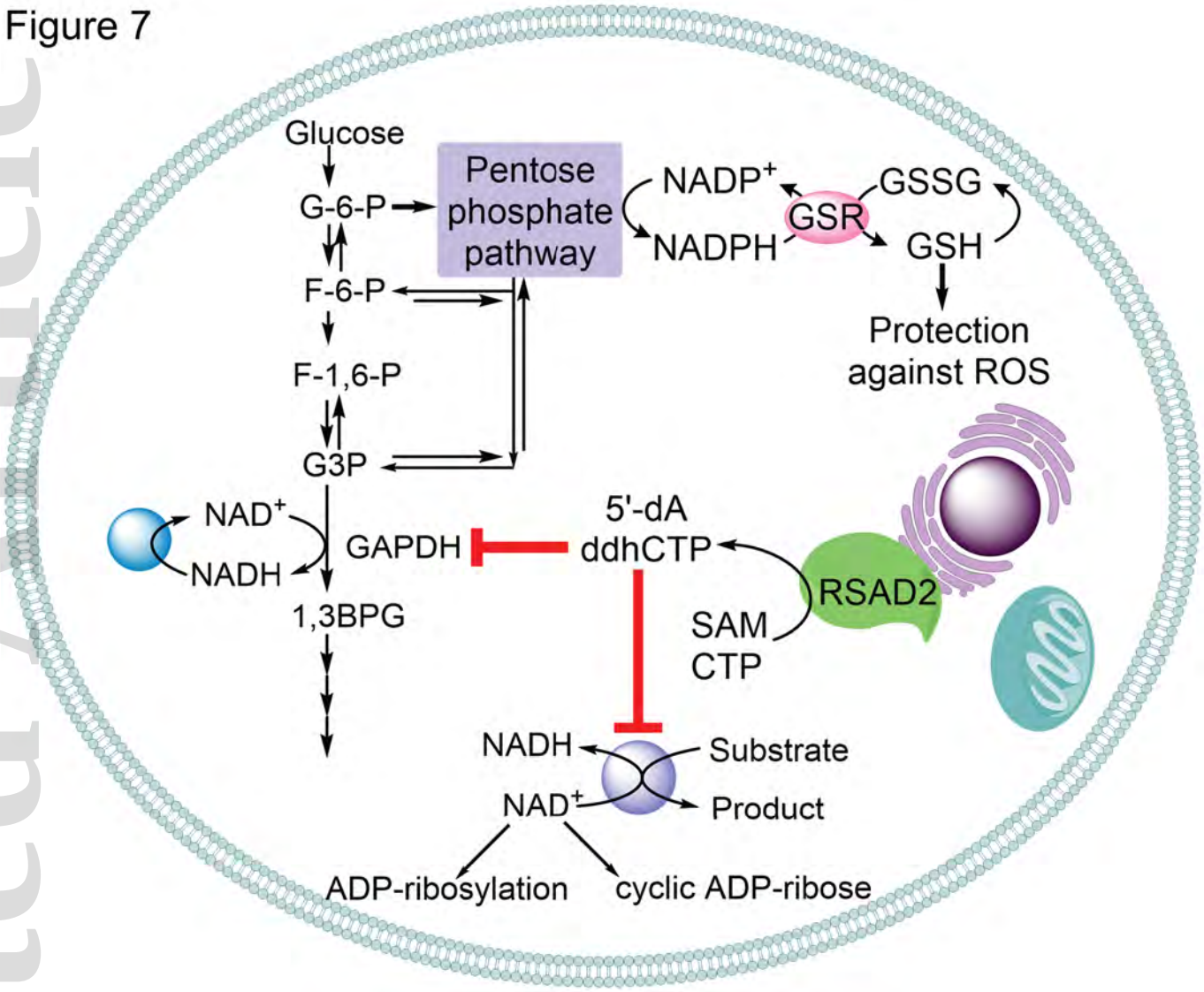


feb2_13778_f7.tif